Trial Production and Experiments of Linear Actuator with HTS Bulk Secondary

doi: 10.1109/77.920240

Trial Production and Experiments of Linear Actuator with HTS Bulk Secondary

R. Muramatsu, S. Sadakata, M. Tsuda, A. Ishiyama

Abstract— **To investigate characteristics of a linear actuator with high-temperature superconducting (HTS) bulk secondary, a short secondary type linear actuator has been designed and constructed. The actuator is comprised of an YBCO bulk secondary (mover) and copper windings with iron core (primary). A zero-field-cooled bulk located at the center of the actuator plays a role of generating thrust, while four field-cooled (trapped field) bulks are used for levitation and guidance of the secondary. We measured the starting thrust force and magnetic field distribution in the air gap. We developed a simulation program based on the finite element method (FEM) taking the voltage-current (*E-J*) characteristics of the bulk into consideration to investigate electromagnetic behaviors within the bulk exposed to a time-varying magnetic field. Agreement between experiment and simulation is good, and it validates the simulation program and the presented assumptions in the numerical approach. Using the simulation program, we investigated the dependency of n-value and critical current density of the bulk material on the magnetic flux density in the air gap and the starting thrust force. Supercurrent density within the bulk is a key factor for the magnetic flux density and the thrust force.**

I. Introduction

It is expected that HTS bulk materials will be applied to various electric devices such as motors, flywheels and fault current limiters. Some rotating machines such as hysteresis, reluctance and synchronous motors have been constructed and demonstrated [1], [2]. We have constructed a linear actuator with an HTS bulk as secondary. To improve the characteristics of the linear actuator, it is very important to investigate the electromagnetic behavior of the linear actuator, especially within the bulk. For this reason, the starting thrust force and the magnetic field distribution in the air gap between the primary and secondary were measured. A simulation based on the FEM taking *E-J* characteristic of the bulk material into consideration has been developed. The time-dependent electromagnetic behavior of cylindrical HTS bulk in a model fault current limiter has been evaluated by the same simulation technique and good agreement between analysis and experiment has been obtained [3]. The computed magnetic field distribution in the air gap and the starting thrust force are compared with experimental data. We also investigated the dependences of the critical current density and n-value in the HTS bulk on the magnetic field distribution in air gap and the starting thrust force, using zero-field-cooled bulk sample.

Manuscript received September 19, 2000.

R. Muramatsu, S. Sadakata, M. Tsuda, and A. Ishiyama are with the Department of Electrical, Electronics and Computer Engineering, Waseda University, 3-4-1 Ohkubo, Shinjyuku-ku, Tokyo 169-8555, Japan (e-mail: atsushi@mn.waseda.ac.jp).

II. The Model Actuator

A schematic drawing of a model linear actuator used in the experiments is shown in Fig. 1. The primary and the secondary of the linear actuator are composed of copper windings with iron core and HTS bulks, respectively. The specifications of the linear actuator are listed in Table 1. As shown in Fig. 1, permanent magnets, the same pole in longitudinal direction and alternating poles of N and S in transverse direction, are located at both sides of the primary windings to levitate and guide the secondary. Two types of HTS bulk were used in the linear actuator. A zero-field-cooled HTS bulk plate is located at the center of the secondary to generate thrust, and field-cooled bulks located above the permanent magnets play a role of levitation and guidance of the secondary. The magnetic flux density distribution at the top surface of the teeth in the iron core was measured by a Hall probe, and the starting thrust force was measured by a load cell.

III. Numerical Simulation

To simulate the electromagnetic behavior of HTS bulks exposed to a time-varying magnetic field, we developed a computer program based on the two-dimensional FEM, taking the *E-J* characteristic of the bulk material into account. The governing equation derived from Maxwell's equation and the *E-J* characteristic are as follows:

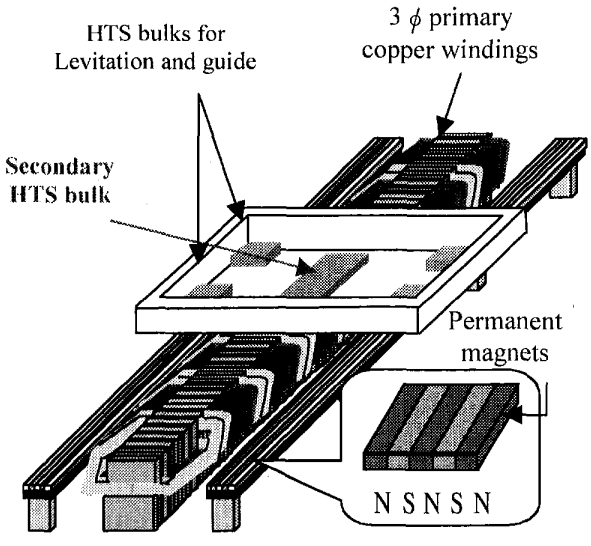

Fig. 1. Experimental setup of linear actuator.

1051-8223/01$10.00 © 2001 IEEE

TABLE I
SPECIFICATIONS OF LINEAR ACTUATOR

Primary (copper winding)		
pole pitch	[mm]	84
number of turns		50
resistance	[Ω]	0.8
Secondary (HTS bulk)		
length	[mm]	84
width	[mm]	47
thickness	[mm]	3
Levitating HTS bulk		
length	[mm]	25
width	[mm]	25
thickness	[mm]	5

$$\frac{\partial}{\partial x}\left(\frac{1}{\mu}\frac{\partial A_z}{\partial x}\right)+\frac{\partial}{\partial y}\left(\frac{1}{\mu}\frac{\partial A_z}{\partial y}\right)=-J_0+J_{SC} \tag{1}$$

$$E=E_C\left(\frac{J_{SC}}{J_C}\right)^n \tag{2}$$

where A_z is the magnetic vector potential in the z direction; μ is the permeability; J_0 is the exciting current density in the primary windings; J_{SC} is the supercurrent density; J_C is the critical current density; and E_C is the critical electric field that defines the critical current density, J_C. We adopt a current sheet approximation for the primary current and the Newton-Raphson method to solve this non-linear problem. The numerical model of the linear actuator is shown in Fig. 2. HTS bulk plate for the secondary, with a length that is equal to the pole pitch τ, is located above the primary. At the vertical lines on both sides of the primary, a periodical boundary condition is adopted. The current sheet, defined as follows, is located on the surface of the primary core.

$$I_s=J_s\sin 2\pi\left(\frac{t}{T}-\frac{x}{2\tau}\right) \tag{3}$$

$$J_s=\frac{6\sqrt{2}K_w NI_1}{\tau} \tag{4}$$

In (3) and (4), t is time, T is the cycle, and J_s denotes the maximum number of current sheet. K_w is the winding factor, I_1 is the effective primary current, and N is the number of turns per single pole. We assume that the critical current density and n-value are the same in all bulks; the critical current density and n-value are set to be 1×10^8 A/m^2 and 15, respectively.

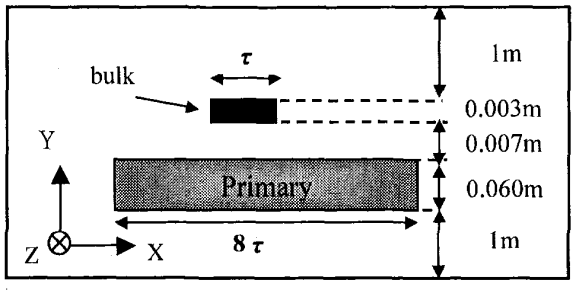

Fig. 2. Analytical model of linear actuator.

IV. RESULTS

A. Magnetic Field Distribution in Air Gap

Experimental and numerical results of the magnetic flux density at primary currents of 0.5 A and 1.0 A are shown in Fig. 3. In Fig. 3, the HTS bulk exists at $-0.042\leqq x\leqq 0.042$. Agreement between the experiment and the simulation is good. Because of shielding supercurrents within the bulk, the magnetic flux density beneath the bulk is relatively small, while the larger magnetic flux density goes around both edges of the bulk. The unsymmetrical measured magnetic flux profile may be caused by heterogeneity of the bulk and experimental errors due to the relative location of the Hall probe to the iron core with teeth and slots. In addition to the unsymmetrical profile, numerical error due to approximations in numerical approach may be the cause for the discrepancy between measured and computed magnetic flux densities.

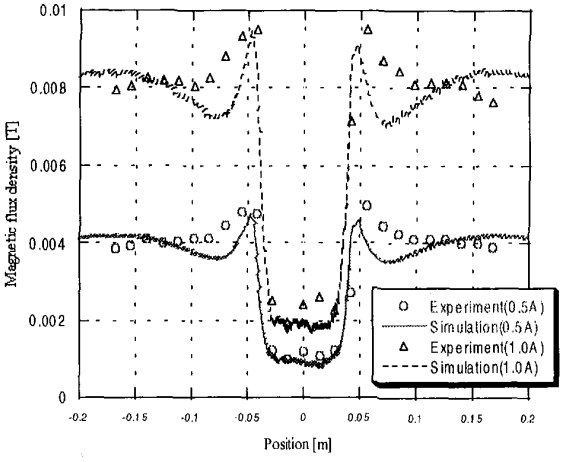

Fig. 3. Magnetic flux density in air gap between the primary and the secondary.

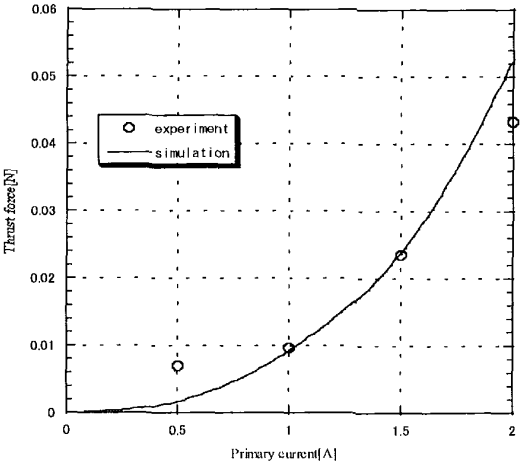

Fig. 4. Starting thrust force.

B. Starting Thrust Force

Because it is difficult to evaluate the thrust force under the operating condition, we measured and investigated the starting thrust force. Even in the starting thrust force, however, the experimental evaluation of a small primary current in the copper windings was very hard because of the small output of the load cell with some noise. The measured and computed thrust force as a function of the primary current in the range of 0 to 2.0 A is shown in Fig. 4. Although the discrepancy between the experiment and the simulation at the primary currents of 0.5 A and 2.0 A are observed, agreement between the experiment and the simulation is good. At a primary current of 0.5 A, experimental error may appear since the output signal from the amplifier of the load cell was particularly small. On the other hand, the thrust force may be reduced at a primary current of 2.0 A because of saturation of the iron core. Considering those errors, we can consider our numerical model and simulation code to be valid.

V. Discussion

The characteristics of linear actuators, such as thrust force in the air gap and stability, depend on electromagnetic behaviors, especially supercurrent distribution within the bulk. It is very important to investigate such dependence for improving the characteristics of linear actuators. Therefore, we investigated the influence of critical current density and n-value of the HTS bulk on the characteristic of the linear actuator. The starting thrust force and the magnetic field distribution in the air gap were evaluated numerically as functions of the critical current density and n-value. Note that the dependency of magnetic flux density on the critical current density and n-value is ignored in the simulation.

The analytical results of magnetic flux density at the primary current of 1 A as functions of n-value and critical current density are shown in Figs. 5 and 6, respectively. Any big differences of the magnetic flux density, however, are not observed in both figures. It can be considered from this result that the magnitude of critical current density and n-value, at least, are not the main cause for the numerical errors in the simulation of Figs. 3 and 4. The numerical results in Figs. 5 and 6 imply that the characteristics of a linear actuator with an HTS bulk secondary may be almost independent of the critical current density and n-value of the HTS bulk in the case that the primary is comprised of copper windings; this means that the primary current is restricted to be small. In order to clarify the dependency of the magnetic flux density in air gap on the critical current density and n-value, we assume that the primary windings are composed of superconducting wires and the primary current is 10 A. The computed results of magnetic flux density as functions of n-value and the critical current density are shown in Figs. 7 and 8, respectively. In Fig. 7, the magnetic field distribution depends on n-value; the magnetic flux density beneath the bulk ($-0.042 \leqq x \leqq 0.042$) increases with n-value. This means that the magnetic flux density with the opposite sign to that of the primary current generated by supercurrent within the bulk,

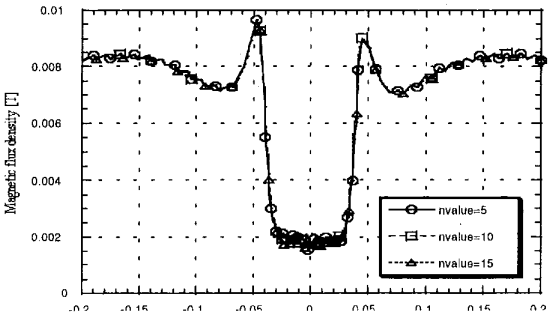

Fig. 5. Dependency of magnetic flux density on n-value of HTS bulk (primary current:1 A).

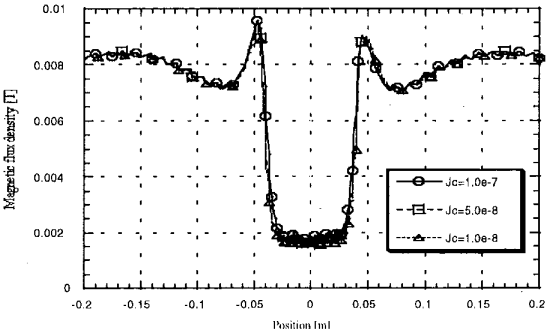

Fig. 6. Dependency of magnetic flux density on critical current density of HTS bulk (primary current:1 A).

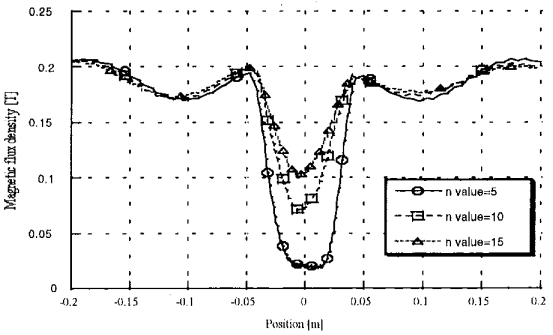

Fig. 7. Dependency of magnetic flux density on n-value of HTS bulk (primary current:10 A).

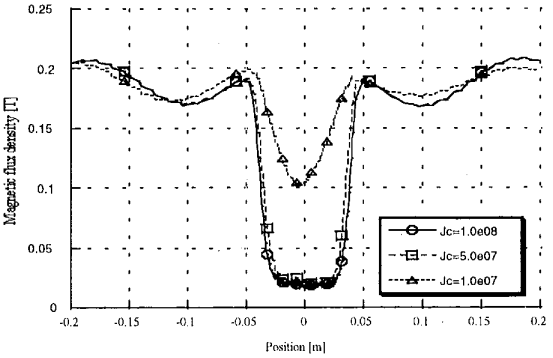

Fig. 8. Dependency of magnetic flux density on critical current density of HTS bulk (primary current:10 A).

decreases with n-value; the larger n-value, the lower supercurrent density within the bulk. The relationship between n-value and the supercurrent density is schematically shown in Fig. 9. In Fig. 9, *Jc*, *Ec* and *Eo* are the critical current density, the induced electric field within bulk and the criterion of electric field for *Jc*, respectively. The slope of the *E-J* curve above *Jc* becomes steeper with n-value. Therefore, when an electric field is induced within the bulk, the supercurrent density of the bulk with small n-value is larger than that of large n-value. In Fig. 8, the magnetic flux density beneath the bulk decreases with critical current density and its tendency is conspicuous between 1×10^7 A/m^2 and 5×10^7 A/m^2. The higher critical current density generates the smaller supercurrent region and the steeper slope of magnetic flux density beneath both edges of the bulk.

The dependence of n-value and *Jc* on the starting thrust force is also investigated numerically. The computed results of the thrust force at the primary current of 10 A as functions of n-value and critical current density are shown in Figs. 10 and 11, respectively. As seen in Figs. 10 and 11, the thrust force increases with n-value and decreases with *Jc*, and the influence of *Jc* on the thrust force is much greater than that of n-value. The results imply that the supercurrent density and the supercurrent distribution are very important for the thrust force; the larger the supercurrent region, the larger the thrust force.

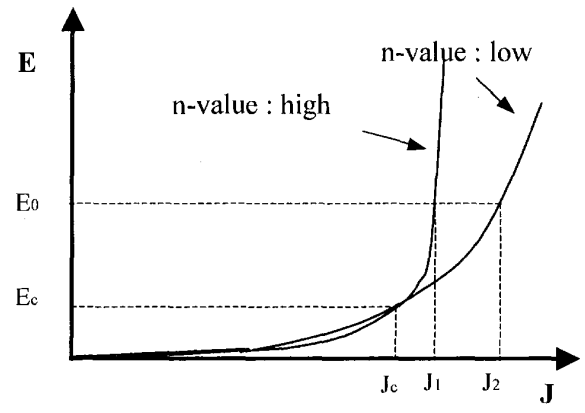

Fig.9. *E-J* characteristics.

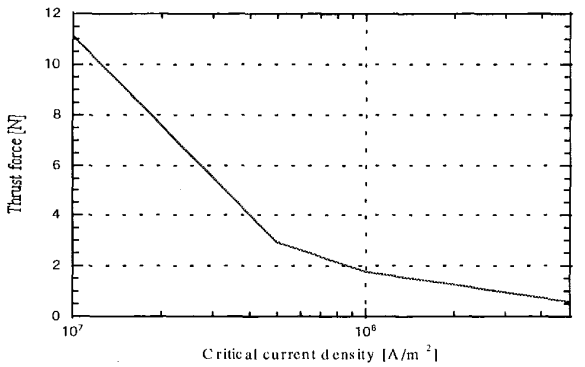

Fig. 10. Dependency of thrust force on critical current density of HTS bulk (primary current : 10 A).

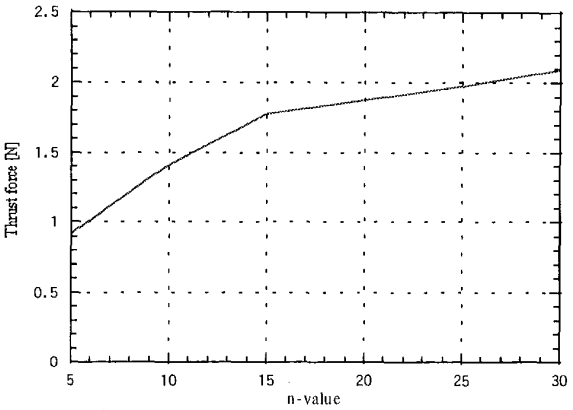

Fig. 11. Dependency of thrust force on n-value of HTS bulk (primary current : 10 A).

Based on the above numerical results of magnetic flux density and thrust force, we can consider that larger n-value and lower critical current density are preferable for the linear actuator.

VI. Summary

We designed and constructed a linear actuator with HTS bulk secondary. Starting thrust force and magnetic field distribution in the air gap were measured in the model linear actuator. A simulation program based on the FEM considering the *E-J* characteristic was developed to evaluate the electromagnetic behavior within the HTS bulk exposed to a traveling external magnetic field. Computed magnetic flux density and starting thrust force were compared with experiments. Agreement between experiments and analyses is good, and it validates the simulation program and assumptions in the numerical approach. Using the simulation program, we investigated the dependency of n-value and critical current density of the bulk on the magnetic flux density and the thrust force. The thrust force depends on the supercurrent density and larger n-value and lower critical current density are preferable for the linear actuator using zero-field-cooled HTS bulk secondary. For next investigation of HTS linear actuators, we are constructing a linear synchronous actuator using trapped field bulk secondary with copper damper windings.

References

[1] L. K. Kovalev et al., "Hysteresis and reluctance electric machines with bulk HTS rotor elements," *IEEE Trans. on Appl. Supercond.*, vol. 9, no. 2, pp. 1261-1264, 1999

[2] L. K. Kovalev, K. V. Ilushin, V. T. Pankin, K. L. Kovalev, et al., "Hysteresis and reluctance electric machines with bulk HTS elements recent results and future development," *Applied Superconductivity,Spain.* vol. 1 , Proceeding of EUCAS 1999, the Fourth European Conference on Applied Superconductivity, pp. 1037-1042, Sept.,1999

[3] J. Nakatsugawa, et al., "Magnetic characteristics of a high-Tc superconducting cylinder for magnetic shielding type superconducting fault current limiter,"*IEEE Trans. on Appl.* Supercond., vol. 9 , no. 2, pp. 1373-1376, 1999